

Communication

Hydrogen-Induced Microstructure Changes in Zr/Nb Nanoscale Multilayer Structures

Roman Laptev ^{1,*}, Ekaterina Stepanova ¹, Anton Lomygin ¹, Dmitriy Krotkevich ¹, Alexey Sidorin ² and Oleg Orlov ²

¹ Division for Experimental Physics, National Research Tomsk Polytechnic University, Tomsk 634050, Russia; enstepanova@tpu.ru (E.S.); adl4@tpu.ru (A.L.); dgk7@tpu.ru (D.K.)

² Dzhelepov Laboratory of Nuclear Problems, Joint Institute for Nuclear Research, Dubna 141980, Russia; sidorina@jinr.ru (A.S.); orlov@jinr.ru (O.O.)

* Correspondence: laptevrs@tpu.ru; Tel.: +7-913-852-3733

Abstract: Zr/Nb nanoscale multilayer coatings (NMCs) were studied after hydrogenation in a gaseous environment at 400 °C. The hydrogen distribution and content were determined by pressure and hydrogenation time. Increasing the pressure from 0.2 to 2 MPa resulted in different hydrogen distribution within the Zr/Nb NMCs, while the concentration remained constant at 0.0150 ± 0.0015 wt. %. The hydrogen concentration increased from 0.0165 ± 0.001 to 0.0370 ± 0.0015 wt. % when the hydrogenation time was extended from 1 to 7 h. The δ -ZrH hydride phase was formed in the Zr layers with Zr crystals reorienting towards the [100] direction. The Nb(110) diffraction reflex shifted towards smaller angles and the interplanar distance in the niobium layers increased, indicating significant lateral compressive stresses. Despite an increase in pressure, the nanohardness and Young's modulus of the Zr/Nb NMCs remained stable. Increasing the hydrogen concentration to 0.0370 ± 0.0015 wt. % resulted in a 40% increase in nanohardness. At this concentration, the relative values of the Doppler broadening variable energy positron annihilation spectroscopy (S/S_0) increased above the initial level, indicating an increase in excess free volume due to hydrogen-induced defects and changes. However, the predominant positron capture center remained intact. The Zr/Nb NMCs with hydrogen content ranging from 0.0150 ± 0.0015 to 0.0180 ± 0.001 wt. % exhibited a decrease in the free volume probed by positrons, as demonstrated by the Doppler broadening variable energy positron annihilation spectroscopy. This was evidenced by opposite changes in S and W ($S \downarrow, W \uparrow$). The microstructural changes are attributed to defect annihilation during hydrogen accumulation near interfaces with the formation of hydrogen–vacancy clusters and hydrides.

Keywords: nanoscale multilayer coatings; hydrogenation; microstructure; positron annihilation; nanohardness; hydrogen-induced defects



Citation: Laptev, R.; Stepanova, E.; Lomygin, A.; Krotkevich, D.; Sidorin, A.; Orlov, O. Hydrogen-Induced Microstructure Changes in Zr/Nb Nanoscale Multilayer Structures. *Metals* **2024**, *14*, 452. <https://doi.org/10.3390/met14040452>

Academic Editor: Babak Shalchi Amirkhiz

Received: 7 March 2024

Revised: 4 April 2024

Accepted: 9 April 2024

Published: 12 April 2024



Copyright: © 2024 by the authors. Licensee MDPI, Basel, Switzerland. This article is an open access article distributed under the terms and conditions of the Creative Commons Attribution (CC BY) license (<https://creativecommons.org/licenses/by/4.0/>).

1. Introduction

Nanoscale multilayers enhance the physical and chemical attributes of materials, such as resistance to corrosion, scratching, radiation, and electrical conductivity. They also improve tensile strength, toughness, and other critical characteristics, making them highly versatile across different industries [1,2]. Nanoscale multilayer coatings (NMCs) used in nuclear and space technology applications may undergo hydrogen-induced processes that alter their microstructure and cause embrittlement [3–8]. To mitigate the impact of hydrogen on nanoscale multilayer structures, internal structural analysis after hydrogenation is required. In pure metals, hydrogen bonds in the following general ways: at low concentrations, hydrogenation causes lattice expansion; at intermediate concentrations, hydrogen atoms form complexes with material atoms; and at high concentrations, hydrogen injection results in a large number of defects in the material [9]. Important factors influencing hydrogen distribution for nanoscale multilayer materials include the presence of interfaces where considerable amounts of hydrogen might concentrate [10–13].

According to Vidur et al.'s thermodynamic model, hydrogen preferentially accumulates in the β -Zr phase of zirconium–niobium alloys, resulting in the decomposition of the substable β -Zr phase and the redistribution of hydrogen to adjacent Zr and Nb interfaces [1]. It is worth noting that for coatings with substantial single-layer thicknesses (50–100 nm), the structural distribution of the coating remains unchanged even if the surface is directly exposed to protons. Protons degrade the coating interface in coatings with thin monolayer thicknesses of 10–25 nm, preserving hydrogen. Proton radiation does not cause serious material damage or alter the structure of the coating. The coating becomes more ductile and less brittle due to the buildup of hydrogen–vacancy complexes, which decreases its hardness. These findings suggest that nanoscale multilayer coatings of Zr/Nb are a possible hydrogen-tolerant material [14,15]. Further investigation into microstructural changes following hydrogen induction is crucial for enhancing the coating production process and material attributes.

The investigation of hydrogen embrittlement is examined with respect to the distinct characteristics of Zr and Nb separately. Zirconium alloys are the preferred choice for nuclear reactor claddings due to their proven resistance to radiation, corrosion, and low neutron absorption. The addition of niobium to the alloys further enhances their resistance to oxidation and corrosion [16,17]. Ion irradiation causes ions to aggregate between the Zr matrix and Nb precipitate grain boundaries, resulting in a less severe increase in the brittleness of NMCs based on these metals, without compromising their hardness [18]. Zirconium has a low solid solubility limit for hydrogen and is highly susceptible to hydrogen embrittlement. The alloy susceptibility to hydrogen absorption at high temperatures and under high radiation damage is a significant factor [19]. Niobium can be used as a layer for shielding zirconium due to its remarkable oxidation resistance; moreover, niobium is not easily deformed, even in high-temperature operations [20]. However, Nb is more susceptible to hydrogen penetration, and its accumulation can cause significant deformation in this layer [21,22]. When using niobium in nanoscale multilayer systems, it is also necessary to reduce lattice swelling due to hydrogen accumulation. The pressure and duration of hydrogenation can affect hydrogen concentration and distribution, as well as cause microstructural changes in multilayer coatings; therefore, its study is the aim of this research.

2. Materials and Methods

The Zr/Nb NMCs were fabricated through a magnetron sputtering process utilizing a specialized apparatus developed at the Weinberg Research Center of Tomsk Polytechnic University. The process involved fixing single-crystalline silicon substrates oriented along the (111) direction inside an experimental chamber equipped with an axial rotation system. During the coating process, an argon (Ar) atmosphere was maintained at an operating pressure of 0.3 Pa, while the residual pressure within the chamber was kept at 0.002 Pa. Before coating, the substrates underwent a 30 min cleaning process using Ar ions at a voltage of 2.5 kV and an ion current of 2.5 mA. The coating was executed using two balanced magnetron sputtering systems by APEL-M-5PDC power supply (Applied Electronics, Tomsk, Russia) [23,24]. The resulting Zr/Nb NMCs samples comprised alternating layers of Zr and Nb, each with a thickness of 50 nm (referred to as Zr/Nb50 NMCs). The total thickness of the coating for each sample was $1.1 \pm 0.2 \mu\text{m}$. The structure of NMCs with different thicknesses of individual layers obtained by this method under the conditions mentioned above is described in detail in works [14,15].

In situ diffraction research was performed using a Shimadzu XRD-7000S diffractometer (Kyoto, Japan, coupled with an Anton Paar HTK 2000N high-temperature chamber) [25]. The samples were resistively heated with a platinum plate under a vacuum of 10^{-3} Pa. The heating process was carried out linearly in 20 °C increments up to a maximum temperature of 700 °C. Registration was performed using a high-speed 1280-channel OneSight detector within the 30.4–47.5° range with one-minute exposure. The in situ diffraction study clearly showed that no crystalline phases or intermetallic compounds formed within the coatings during the linear heating process in vacuum conditions up to 400 °C. The diffraction reflec-

tions corresponding to Zr(002) and Nb(110) remained clearly distinguishable throughout the heating process, as shown in Figure 1.

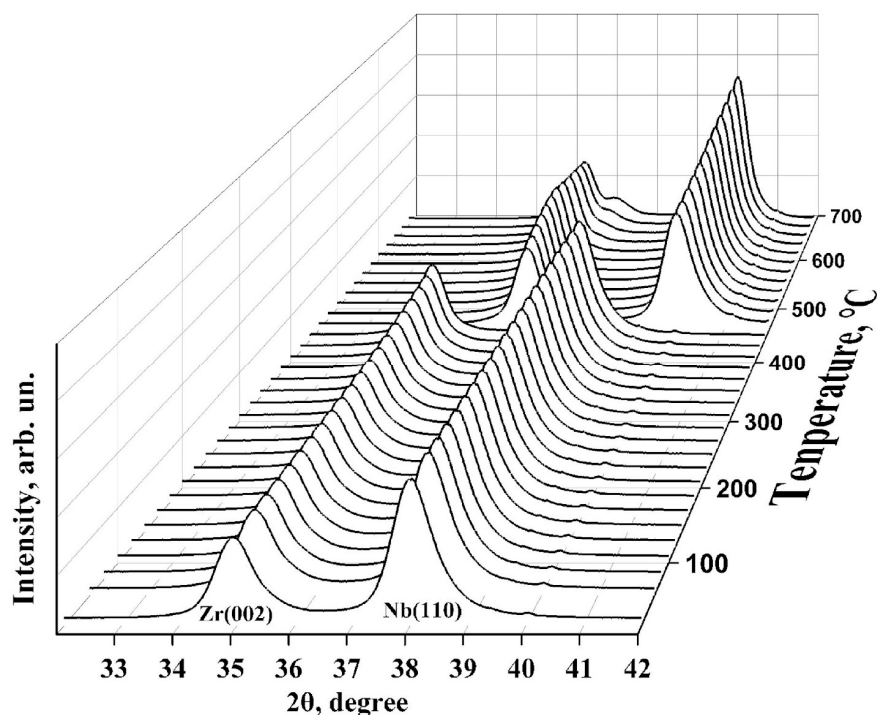


Figure 1. In situ diffraction patterns obtained during linear heating of Zr/Nb50 NMCs in vacuum.

It can be seen from the figure that heating leads to a simultaneous abrupt shift of diffraction reflexes towards higher angles by more than 2° in the temperature range above 450°C , which is related to the delamination of the coatings from the substrate. These effects are associated with variations in the thermal properties of each constituent of the coating–substrate system (Zr, Nb, and Si).

The Zr/Nb50 samples were hydrogenated using the Sieverts method with an automated Gas Reaction Controller LPB. The hydrogen used had a purity exceeding 99.9995% and was generated by a Proton HyGen 200 hydrogen generator. A hydrogenation temperature of 400°C (with a heating rate of $6^\circ\text{C}/\text{min}$) was chosen following analysis of the diffraction studies to prevent system delamination. After absorption, cooling was also performed in a hydrogen medium at residual pressure at a rate of $5^\circ\text{C}/\text{min}$. The different hydrogen distribution was predominantly specified by changing the pressure from 0.2 to 2 MPa for a three-hour exposure, and the hydrogen content was mainly defined by the hydrogenation time from 1 to 7 h at a maximum pressure of 2 MPa. The LECO RHEN602 analyzer was used to quantify the absolute hydrogen concentration in Zr/Nb50 NMCs; it should be noted that initial samples had a hydrogen concentration not exceeding 0.001 wt. %.

Using glow-discharge optical emission spectrometry, the layer-by-layer distribution of the Zr and Nb elements was examined. The GD-OES technique has a low chemical element detection limit and a high depth resolution. Using a 4 mm anode and the following parameters, the depth profiling was performed on a GD-Profilier 2 spectrometer (Jobin Yvon Emission Horiba Group, Palaiseau, France): 650 Pa of pressure, 40 W of power, 1 kHz of frequency, and 25% duty cycle.

The fine structure of the samples was thoroughly analyzed by transmission electron microscopy using a JEM-2100F microscope (JEOL, Akishima, Japan). The specimens were prepared by ion thinning using an Ion Slicer EM-09100IS (JEOL, Akishima, Japan). The etching angle ranged from 1.5 to 4 degrees with an acceleration voltage of 8 kV, and argon was used as the working gas during specimen preparation. Nanohardness and Young's modulus were determined using an indentation/scratch tester NHT 50-183/NST 50-146 (CSM Instruments,

Peuseux, Switzerland) with a load of 5 mN and a dwell time of 30 s. Additionally, Doppler broadening spectroscopy (DBS) was performed at the Dzhelepov Laboratory of Nuclear Problems (Joint Institute for Nuclear Research, Dubna, Russia) using a positron beam of various energies ranging from 0.1 to 22 keV. The dependencies S/S_0 and W/W_0 were used for the analysis of Zr/Nb50 NMCs, where S_0 and W_0 represent DBS parameters before hydrogenation, and S and W represent DBS parameters after hydrogenation.

3. Results

Figure 2 demonstrates the hydrogen sorption curves of Zr/Nb50 NMCs at varying pressures (Figure 2a) and hydrogenation times (Figure 2b). The final value of hydrogen concentration in Zr/Nb50 has a minimal variation when the pressure is adjusted from 0.2 to 2 MPa. However, with an extension of the hydrogenation time from 1 to 7 h at maximum pressure (Figure 2b), the hydrogen content of Zr/Nb50 increases more significantly.

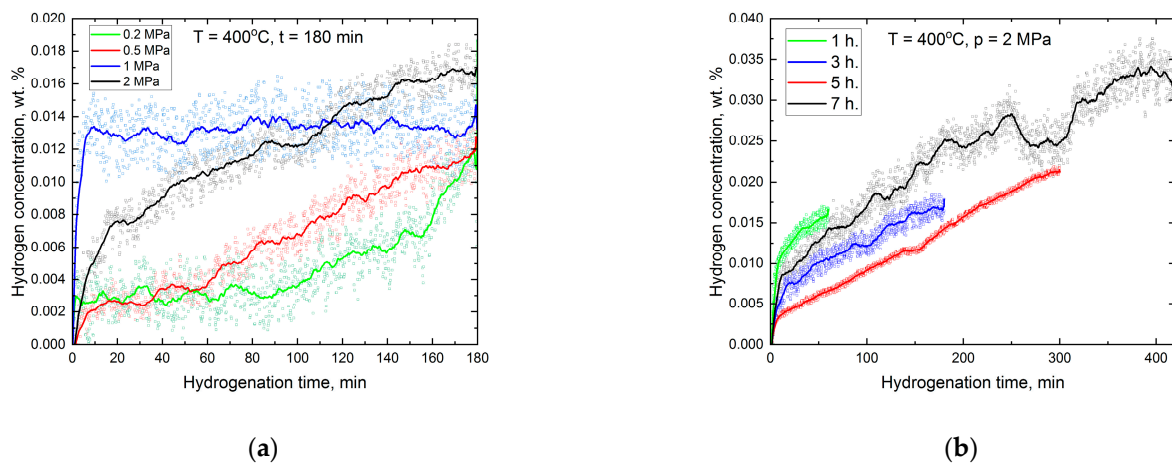


Figure 2. Hydrogen absorption curves of Zr/Nb50 at different pressure (a) and hydrogenation time (b).

The values of hydrogen concentrations obtained by melting in an argon atmosphere for hydrogenated Zr/Nb50 NMCs at different pressures and times are presented in Table 1.

Table 1. Absolute hydrogen concentration in Zr/Nb50 after hydrogenation at a different pressure and time.

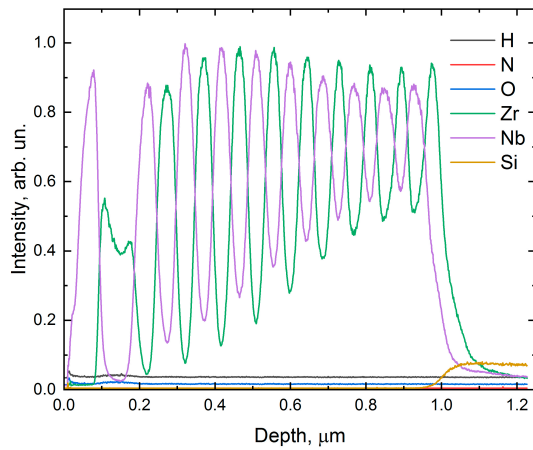
Pressure, MPa	H concentration, wt. %	Time, h	H concentration, wt. %
0.2	0.0143 ± 0.001	1	0.0165 ± 0.001
0.5	0.0149 ± 0.001	3	0.0168 ± 0.001
1	0.0155 ± 0.001	5	0.0180 ± 0.001
2	0.0168 ± 0.001	7	0.0370 ± 0.0015

An increase in the pressure leads to a more uniform hydrogen distribution throughout the Zr/Nb50 NMCs, with an average H concentration of 0.0154 ± 0.001 wt. %. Extending the hydrogenation period from 1 to 7 h results in an increase in hydrogen concentration from 0.0165 ± 0.001 to 0.0370 ± 0.0015 wt. %. This indicates that cooling the samples in a hydrogen atmosphere after high-temperature hydrogenation does not result in increased absorption.

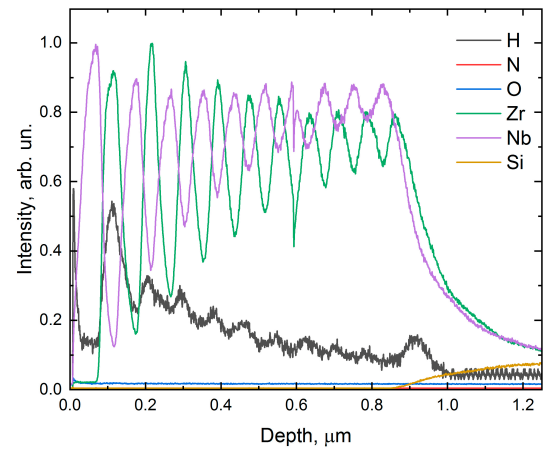
To understand the localization of hydrogen in the Zr/Nb50 NMCs, the depth distribution of the elements was studied using GDOES (Figure 3). Figure 3a represents the elemental distribution profile of the original Zr/Nb50 NMCs, showing the absence of impurities in the samples. Figure 3b–d demonstrate the distribution profiles of the samples hydrogenated at different pressures. Hydrogenation at 0.2 MPa for 3 h results in hydrogen saturation of the first layers of Zr/Nb50 NMCs; as the substrate is approached, a decrease in the intensity of the hydrogen luminescence is observed. Hydrogenation at 1 MPa for

3 h leads to a uniform distribution of hydrogen in the Zr/Nb50 NMCs. When the pressure is increased to 2 MPa, a rise in the hydrogen concentration is observed mainly in the first 10 layers in the Zr/Nb50 NMCs, but the intensity of the hydrogen signal after 10 layers remains at the same level, as in the Zr/Nb50 NMCs hydrogenated at 1 MPa for 3 h.

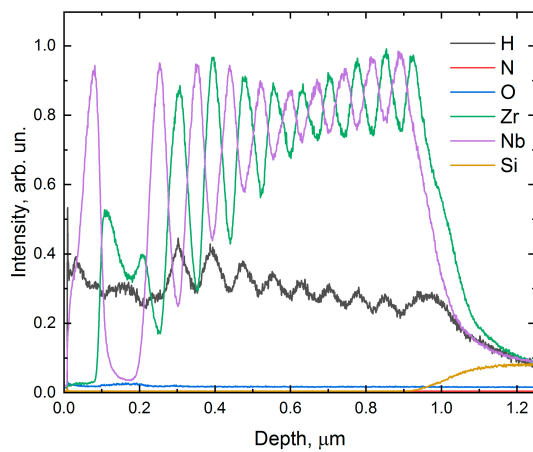
Figure 3d,e show the elemental distribution profiles at different hydrogenation times. With increasing time at high hydrogenation pressure, a rise in the hydrogen signal is observed throughout the Zr/Nb50 NMCs coating. During hydrogenation, there is a tendency for hydrogen to accumulate predominantly in the Zr layers, but, with increasing pressure, there is a tendency for hydrogen to accumulate in the first Nb layer in the form of a solid solution.



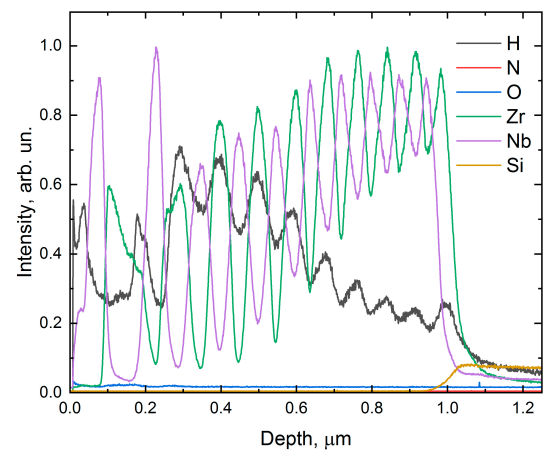
(a)



(b)

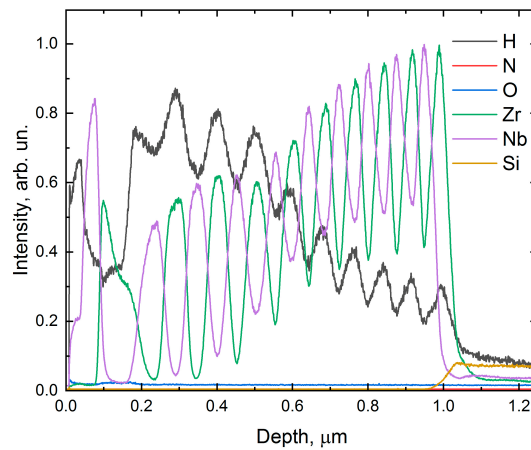


(c)



(d)

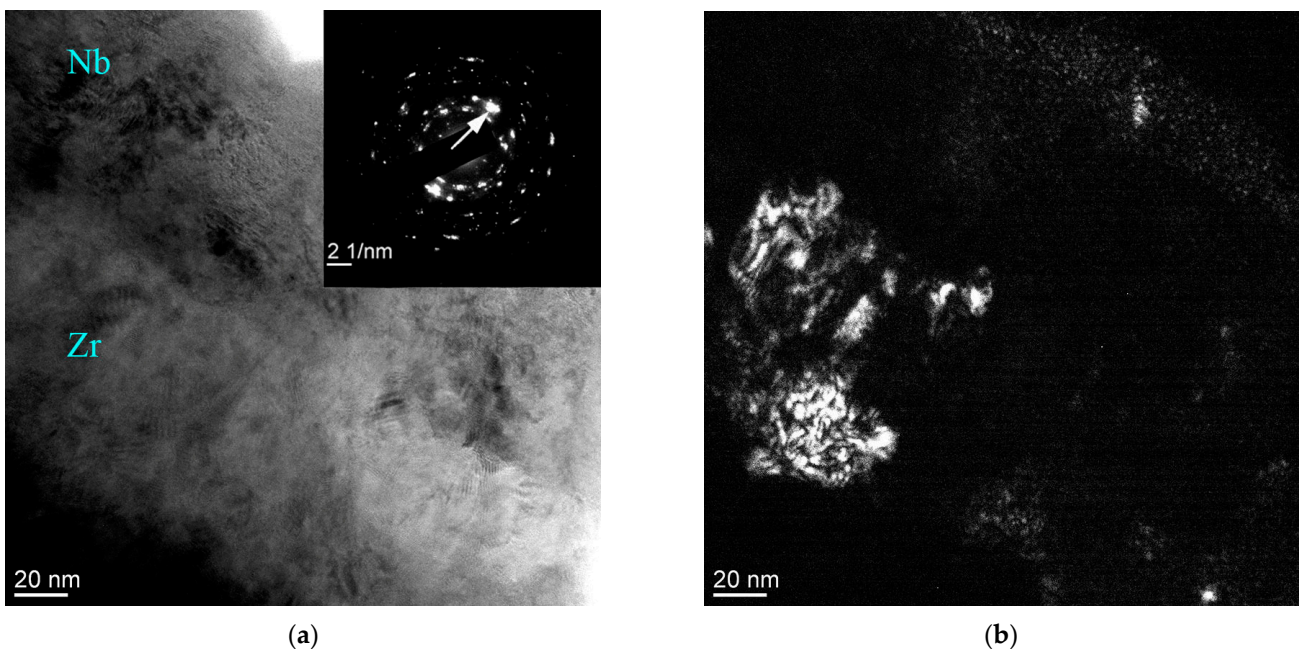
Figure 3. Cont.



(e)

Figure 3. Elemental depth distribution profiles for NMCs Zr/Nb50: (a) initial, (b) hydrogenated at 0.2 MPa and 3 h, (c) hydrogenated at 1 MPa and 3 h, (d) hydrogenated at 2 MPa and 3 h, (e) hydrogenated at 2 MPa and 7 h.

Electron microscopic studies of the sample cross sections of the hydrogenated Zr/Nb50 NMCs have shown that the multilayered structure in all samples, regardless of the final hydrogen concentration, is preserved. Figure 4 shows, as an example, the structure of Zr/Nb50 NMCs after hydrogenation at 400 °C, 2 MPa, and 7 h, because of which the highest hydrogen content was obtained. It can be seen that the samples exhibit a layered structure with alternating layers of zirconium and niobium, the thickness of which was equal to 50 ± 15 nm. In the bulk of each zirconium and niobium layers, nanoscale columnar grains with sizes of 30–50 nm are observed. A significant number of reflections distributed over a circle in the SAED (Figure 4a) obtained for an area of $0.2 \mu\text{m}^2$ indicates the presence of a large number of elements in the structure unit volume and their substantial misorientation. The SAED patterns contained reflections from the different planes of the Zr_α and Nb_β .



(a)

(b)

Figure 4. Typical cross-sectional microstructure of the Zr/Nb50 sample hydrogenated to a concentration of 0.0370 wt. %: bright-field image and corresponding SAED (a), dark-field image in (110) Zr_α reflection (indicated by arrow) (b).

X-ray diffraction studies have shown that hydrogenation, even at small concentrations, leads to a significant change in the appearance of the X-ray diffraction patterns. In this case, regardless of the hydrogenation conditions, the diffraction reflection corresponding to the Zr(002) plane disappears (Figure 5) and the formation of the δ -ZrH hydride phase is observed, as well as the reorientation of Zr crystallites in the [100] direction. The diffraction reflection of Nb(110) shows a significant shift towards smaller angles, resulting in an increase in the corresponding interplanar distance to 2.455 Å. The interplanar distance corresponding to the Nb(110) reflection varies within ± 0.01 Å depending on the saturation modes (see Figure 5). Notable lateral compressive stresses are observed.

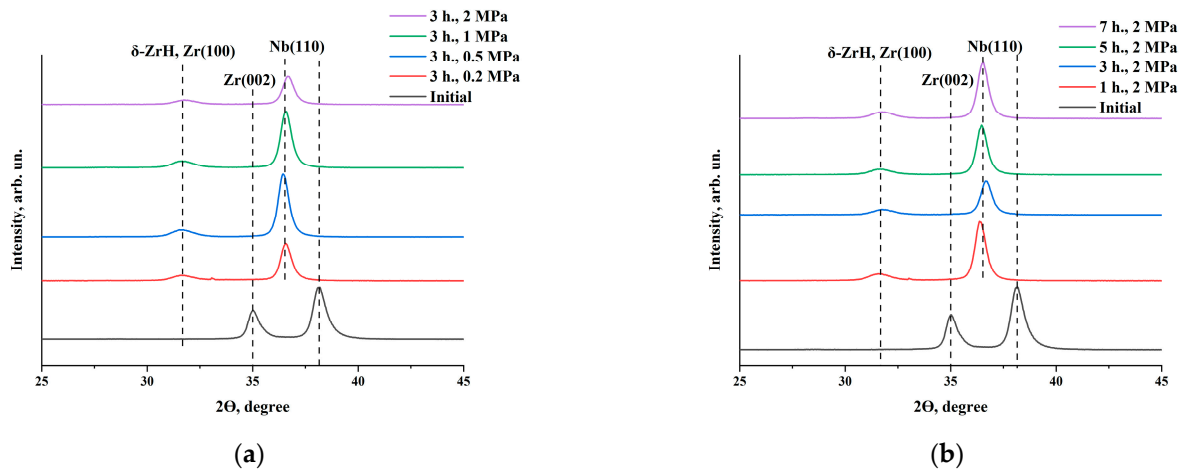


Figure 5. Diffractograms of Zr/Nb50 NMCs obtained for samples saturated with hydrogen at different pressures (a) and different times (b).

Table 2 presents the findings of the nanohardness measurements of Zr/Nb50 at different hydrogenation times.

Table 2. Mechanical properties of Zr/Nb50 with different hydrogen concentrations.

Time, h	H concentration, wt. %	Nanohardness, ± 30 HV	Young Modulus, $\pm 0.1 \times 10^5$, N/mm ²
1	0.0165 ± 0.001	1420	1.2
3	0.0168 ± 0.001	1400	1.3
5	0.0180 ± 0.001	1400	1.3
7	0.0370 ± 0.0015	1520	1.2

The results demonstrate a significant increase in nanohardness when the hydrogen saturation is up to 0.0370 ± 0.0015 wt. %. Vickers nanohardness increases by 40% at a hydrogen concentration of 0.0370 ± 0.0015 wt. %, mainly due to the precipitation of hydrides. However, there is virtually no change in nanohardness when the hydrogen level is altered from 0.0165 ± 0.001 to 0.0180 ± 0.001 wt. % (Table 2). Young modulus, which is approximately 1.3×10^5 N/mm², remains nearly unchanged before and after hydrogenation.

Figure 6 demonstrates the layer-by-layer analysis of DBS in a Zr/Nb50 sample that has been hydrogenated at different pressures. The S/S_0 and W/W_0 profiles undergo significant changes with increasing pressure, but the S values remain below their initial values, which is unusual for the high-temperature hydrogenation of metallic materials [26].

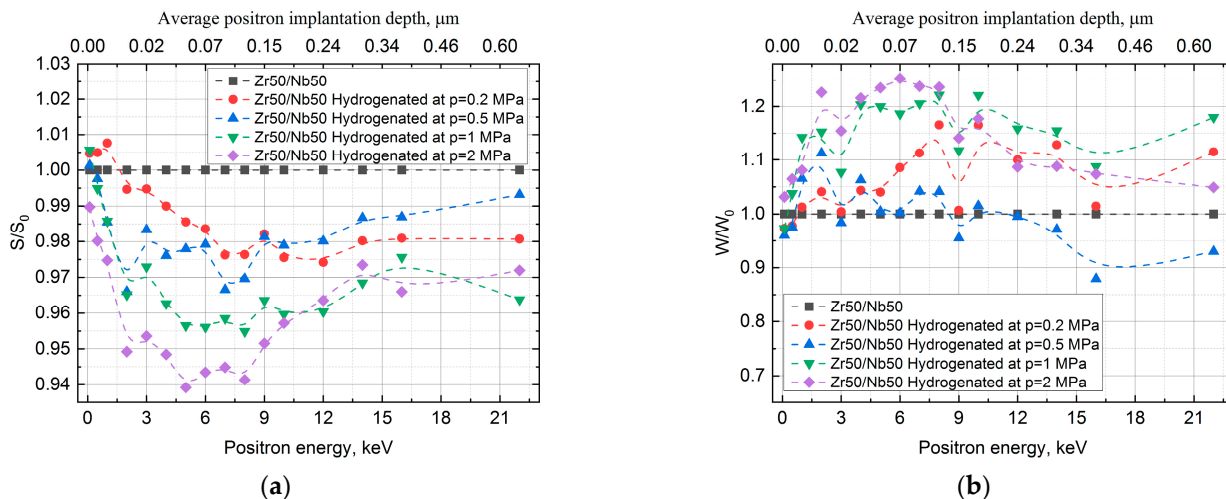


Figure 6. S/S_0 (a) and W/W_0 (b) dependences of positrons of variable energy in hydrogenated Zr/Nb50 NMCs with different pressures.

The accumulation of hydrogen-induced defects, as well as structural-phase transformations, is accompanied by a change in the momentum distribution, primarily resulting in an increase in S values, as the free volume probed by positrons expands. During the high-temperature hydrogenation of metallic materials, vacancy clusters (mV), simple (V-nH), and complex (mV-nH) hydrogen–vacancy clusters are sequentially formed depending on the hydrogen content and phase transitions determined by the hydrogenation conditions, with these defect transitions occurring near the phase boundary [27]. The decrease in S/S_0 parameters (and increase in W/W_0) in Zr/Nb NMCs after hydrogenation is explained by the partial annihilation of defects against the background of hydrogen atoms accumulation in metals lattices with the formation of hydrogen–vacancy complexes near interfaces and hydride formation. Increasing pressure alters the hydrogen distribution in Zr/Nb NMCs; consequently, the hydrogen concentration in the bulk of the layers and at boundaries varies, leading to changes in the relative DBS parameters. However, these dependencies do not imply a change in the positron trapping center; positrons also preferentially annihilate at interfaces.

As the concentration of hydrogen increases, more notable alterations in the relative DBS parameters are noted (Figure 7).

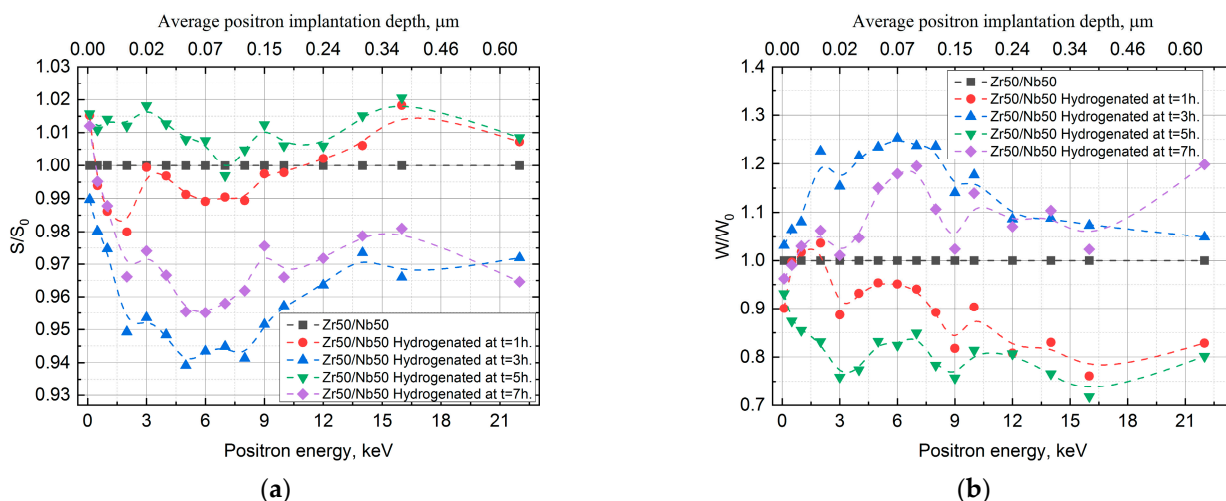


Figure 7. S/S_0 (a) and W/W_0 (b) dependencies of positrons of variable energy in hydrogenated Zr/Nb50 NMCs under maximum pressure at different times.

S/S_0 values are lower than the initial level for Zr/Nb NMCs with hydrogen content ranging from 0.0165 ± 0.001 to 0.0180 ± 0.001 wt. %, and noticeable fluctuations of the corresponding W/W_0 values are observed. This is caused by the intensive formation of hydrides and hydrogen–vacancy complexes, while their structure and distribution are inhomogeneous. At a hydrogen content of 0.0370 ± 0.0015 wt. %, there is an increase in S/S_0 values above the initial level, indicating an increase in excess free volume due to the formation of hydrogen-induced defects and alterations, but the prevailing positron capture center is retained.

4. Conclusions

The hydrogenation of Zr/Nb NMCs, with individual layer thicknesses of 50 nm, was carried out at 400 °C from a gas atmosphere. The hydrogen concentration averaged at 0.0154 ± 0.001 wt. % and was not significantly affected by pressure. However, a tendency for hydrogen accumulation in zirconium layers was observed. Increasing the hydrogenation time from 1 to 7 h at maximum pressure resulted in a significant increase in hydrogen concentration from 0.0165 ± 0.001 to 0.0370 ± 0.0015 wt. %. The Zr layers form a δ -ZrH hydride phase and the Zr crystallites reorient in the [100] direction. The Nb(110) diffraction reflex shifts towards smaller angles and the interplanar spacing in the niobium layers increases due to significant lateral compressive stresses. The nanohardness and Young's modulus of Zr/Nb NMCs remain constant with increasing pressure, likely due to the constant indentation depth and relatively low hydrogen content, which does not exceed 0.0154 ± 0.001 wt. %. However, increasing the hydrogen concentration to 0.0370 ± 0.0015 wt. % results in a significant 40% increase in nanohardness. The relative S/S_0 values of the variable energy positron annihilation pulse distribution increase above the initial level at this concentration. This increase indicates an increase in excess free volume due to the formation of hydrogen-induced defects and alterations. Nevertheless, the prevailing positron trapping center remains unchanged. The momentum distribution of the positron annihilation of variable energy in Zr/Nb NMCs with a hydrogen content ranging from 0.0143 ± 0.001 to 0.0180 ± 0.001 wt. % shows opposite changes ($S \downarrow W \uparrow$), indicating a decrease in the free volume probed by positrons. This decrease is likely due to the partial annealing of defects during the accumulation of hydrogen in metal lattices, resulting in the formation of hydrogen–vacancy complexes near the boundaries and hydrides. The increased resistance of nanosized Zr/Nb multilayers to hydrogenation is, therefore, probably due to the following two effects: vacancies formed in layers close to the Zr/Nb interface are suppressed by the significant relaxation of metal atoms at the interface; and hydrogen forms complexes mainly in zirconium layers close to the interface, increasing the mobility of Zr atoms, which contributes to enhanced defect annihilation. The self-healing of vacancy-type defects resulting from the hydrogenation of nanoscale Zr/Nb multilayers is attributed to these effects.

Author Contributions: Conceptualization, R.L. and A.L.; methodology, E.S.; software, R.L. and O.O.; validation, R.L. and E.S.; formal analysis, A.L., D.K., A.S. and O.O.; investigation, A.L., D.K., A.S. and O.O.; resources, R.L.; A.S.; data curation, A.S. and O.O.; writing—original draft preparation, A.L., E.S. and D.K.; writing—review and editing, R.L. and A.S.; visualization, E.S., A.L. and O.O.; supervision, R.L.; project administration, R.L.; funding acquisition, R.L. All authors have read and agreed to the published version of the manuscript.

Funding: This work was funded by the Russian Science Foundation, research project No. 20-79-10343.

Institutional Review Board Statement: Not applicable.

Informed Consent Statement: Not applicable.

Data Availability Statement: The raw data supporting the conclusions of this article will be made available by the authors on request.

Acknowledgments: The TEM and STEM research was carried out using the equipment of the CSU NMNT TPU, supported by the RF MES project No. 075-15-2021-710.

Conflicts of Interest: The authors declare no conflicts of interest.

References

1. Tuli, V.; Claisse, A.; Burr, P.A. Hydrogen Solubility in Zr–Nb Alloys. *Scr. Mater.* **2022**, *214*, 114652. [[CrossRef](#)]
2. Motta, A.T.; Capolungo, L.; Chen, L.-Q.; Cinbiz, M.N.; Daymond, M.R.; Koss, D.A.; Lacroix, E.; Pastore, G.; Simon, P.-C.A.; Tonks, M.R.; et al. Hydrogen in Zirconium Alloys: A Review. *J. Nucl. Mater.* **2019**, *518*, 440–460. [[CrossRef](#)]
3. Bertolino, G.; Meyer, G.; Perez Ipiña, J. Degradation of the Mechanical Properties of Zircaloy-4 Due to Hydrogen Embrittlement. *J. Alloys Compd.* **2002**, *330–332*, 408–413. [[CrossRef](#)]
4. Bakardjieva, S.; Horak, P.; Vacik, J.; Cannavò, A.; Lavrentiev, V.; Torrìsi, A.; Michalčova, A.; Klie, R.; Rui, X.; Calcagno, L.; et al. Effect of Ar⁺ Irradiation of Ti₃InC₂ at Different Ion Beam Fluences. *Surf. Coat. Technol.* **2020**, *394*, 125834. [[CrossRef](#)]
5. Zinkle, S.J.; Was, G.S. Materials Challenges in Nuclear Energy. *Acta Mater.* **2013**, *61*, 735–758. [[CrossRef](#)]
6. Lu, K.; Singh, S. In-Situ Tem Study of Kr Ion Irradiation Tolerance of Sifeoc Nanocomposite. *SSRN Electron. J.* **2022**. [[CrossRef](#)]
7. Moisy, F.; Sall, M.; Grygiel, C.; Ribet, A.; Balanzat, E.; Monnet, I. Optical Bandgap and Stress Variations Induced by the Formation of Latent Tracks in GaN under Swift Heavy Ion Irradiation. *Nucl. Instrum. Methods Phys. Res. Sect. B Beam Interact. Mater. At.* **2018**, *431*, 12–18. [[CrossRef](#)]
8. Wang, S.; Guo, W.; Wang, H.; Yi, X.; Ge, L.; Sun, Y.; Cheng, L.; Zhang, X.; Yuan, Y.; Cao, X.; et al. Defect Annealing in Heavy-Ion Irradiated Tungsten: Long-Time Thermal Evolution of Saturated Displacement Damage at Different Temperatures. *J. Nucl. Mater.* **2023**, *581*, 154454. [[CrossRef](#)]
9. Sakaki, K.; Yamada, T.; Mizuno, M.; Araki, H.; Shirai, Y. Hydrogen-Induced Vacancy Generation Phenomenon in Pure Pd. *Mater. Trans.* **2002**, *43*, 2652–2655. [[CrossRef](#)]
10. Shukla, S.; Singh, R.N.; Kashyap, Y.S.; Murty, T.N.; Keskar, N.; Roy, T.; Singh, P.; Shukla, M. Anisotropy Study of Hydrogen Diffusion along Different Directions of Zr-2.5%Nb Alloy Pressure Tube Using Neutron Imaging. *J. Nucl. Mater.* **2023**, *580*, 154414. [[CrossRef](#)]
11. Hawes, J.; Warnicke, P.; Burr, P.; Ferreira Sanchez, D.; Grolimund, D.; Partezana, J.; Chiu, Y.-L.; Abolhassani, S. The Speciation of Niobium in the Oxide Layer of an Irradiated Low-Tin ZIRLO Nuclear Material. *Corros. Sci.* **2021**, *190*, 109630. [[CrossRef](#)]
12. Liu, H.; Zhang, J.; Zhou, C.; Sun, P.; Liu, Y.; Fang, Z.Z. Hydrogen Storage Properties of Ti-Fe-Zr-Mn-Nb Alloys. *J. Alloys Compd.* **2023**, *938*, 168466. [[CrossRef](#)]
13. Liaw, L.-J.; Chang, P.-C.; Chen, P.-W.; Liu, Z.-Q.; Liu, S.-Y.; Hsieh, C.-T.; Dhanarajgopal, A.; Chern, M.-Y.; Lo, F.-Y.; Lin, W.-C. Hydrogen-Induced Magnetic and Structural Changes in Pd/Co/Mg Multilayer. *Surf. Interfaces* **2023**, *36*, 102503. [[CrossRef](#)]
14. Laptev, R.; Krotkevich, D.; Lomygin, A.; Stepanova, E.; Pushilina, N.; Kashkarov, E.; Doroshkevich, A.; Sidoren, A.; Orlov, O.; Uglov, V. Effect of Proton Irradiation on Zr/Nb Nanoscale Multilayer Structure and Properties. *Metals* **2023**, *13*, 903. [[CrossRef](#)]
15. Laptev, R.; Stepanova, E.; Pushilina, N.; Svyatkin, L.; Krotkevich, D.; Lomygin, A.; Ognev, S.; Siemek, K.; Doroshkevich, A.; Uglov, V. Distribution of Hydrogen and Defects in the Zr/Nb Nanoscale Multilayer Coatings after Proton Irradiation. *Materials* **2022**, *15*, 3332. [[CrossRef](#)] [[PubMed](#)]
16. Cox, B. Some Thoughts on the Mechanisms of In-Reactor Corrosion of Zirconium Alloys. *J. Nucl. Mater.* **2005**, *336*, 331–368. [[CrossRef](#)]
17. Gómez, A.G.; Ponce, J.P.; Grosse, M.; Soria, S.; Condó, A.; Flores, A.; Schulz, M.; Vizcaíno, P.; Santisteban, J.R. Evaluation of the Delayed Hydrogen Cracking Behavior and the Hydrogen Diffusion Coefficient for Different Microstructures of the Zr-2.5%Nb Alloy. *J. Nucl. Mater.* **2023**, *587*, 154725. [[CrossRef](#)]
18. Sen, H.S.; Polcar, T. Vacancy-Interface-Helium Interaction in Zr-Nb Multi-Layer System: A First-Principles Study. *J. Nucl. Mater.* **2019**, *518*, 11–20. [[CrossRef](#)]
19. Olsson, P.A.T.; Kese, K.; Alvarez Holston, A.-M. On the Role of Hydrogen Filled Vacancies on the Embrittlement of Zirconium: An Ab Initio Investigation. *J. Nucl. Mater.* **2015**, *467*, 311–319. [[CrossRef](#)]
20. Serra, E.; Zola, D.; Scotini, A.; Scaglione, S. Hydrogen and Deuterium Permeation on Niobium Coated by Ultrathin Pd25%Ag for Tritium Recovery in EU DEMO. *Fusion Eng. Des.* **2023**, *193*, 113838. [[CrossRef](#)]
21. Liu, Q.; Jin, W.; Chen, X.; Mao, X.; Liang, C.; Chen, C. The Effects of Hydrogen-Induced Lattice Distortion and Nb-D Formation on Its Permeation through Niobium. *Int. J. Hydrogen Energy* **2021**, *46*, 39932–39941. [[CrossRef](#)]
22. Liu, X.; Liu, N.; Noël, J.J.; Shoosmith, D.W.; Chen, J.; Hou, B. The Influence of Hydrogen Permeation on the Protection Performance of the Cu Coating of Nuclear Waste Containers. *Corros. Sci.* **2023**, *221*, 111314. [[CrossRef](#)]
23. Sidelev, D.V.; Yurjev, Y.N.; Krivobokov, V.P.; Erofeev, E.V.; Penkova, O.V.; Novikov, V.A. The Oxygen-Deficient TiO₂ Films Deposited by a Dual Magnetron Sputtering. *Vacuum* **2016**, *134*, 29–32. [[CrossRef](#)]
24. Yurjev, Y.N.; Zaitcev, D.A.; Sidelev, D.V.; Tupikova, O.S. Effect of Magnetic Field Configuration of Dual Magnetron on Carbon Based Films Properties. *Adv. Mater. Res.* **2014**, *1040*, 721–725. [[CrossRef](#)]
25. Syrtanov, M.; Garanin, G.; Kashkarov, E.; Pushilina, N.; Kudiiarov, V.; Murashkina, T. Laboratory X-ray Diffraction Complex for In Situ Investigations of Structural Phase Evolution of Materials under Gaseous Atmosphere. *Metals* **2020**, *10*, 447. [[CrossRef](#)]

26. Bordulev, I.; Kudiiarov, V.; Svyatkin, L.; Syrtanov, M.; Stepanova, E.; Čížek, J.; Vlček, M.; Li, K.; Laptev, R.; Lider, A. Positron Annihilation Spectroscopy Study of Defects in Hydrogen Loaded Zr-1Nb Alloy. *J. Alloys Compd.* **2019**, *798*, 685–694. [[CrossRef](#)]
27. Laptev, R.S.; Kudiiarov, V.N.; Bordulev, Y.S.; Mikhaylov, A.A.; Lider, A.M. Gas-Phase Hydrogenation Influence on Defect Behavior in Titanium-Based Hydrogen-Storage Material. *Prog. Nat. Sci. Mater. Int.* **2017**, *27*, 105–111. [[CrossRef](#)]

Disclaimer/Publisher’s Note: The statements, opinions and data contained in all publications are solely those of the individual author(s) and contributor(s) and not of MDPI and/or the editor(s). MDPI and/or the editor(s) disclaim responsibility for any injury to people or property resulting from any ideas, methods, instructions or products referred to in the content.